American Mineralogist, Volume 92, pages 1316–1324, 2007

Al,Si order in albite and its effect on albite dissolution processes: A Monte Carlo study

Li Zhang and Andreas Lüttge*

Department of Earth Science, Rice University, 6100 Main Street, Houston, Texas 77005, U.S.A.

Abstract

The role of (Al,Si) disorder in the kinetics of albite dissolution is explored through parameterized Monte Carlo methods. Two dissolution mechanisms—multilayer leaching and single-layer retreat—were tested on 48 albite test configurations. In simulations involving multilayer leaching, dissolution rates increased with decreasing long-range order (LRO). We observed a fivefold maximum increase in dissolution rate tied to (Al,Si) disordering, roughly equivalent to that accompanying a decrease of 1.4 pH units at pH 1–5. This increase in rate due to disordering in albite is similar to that observed from compositional variation in plagioclase feldspars (An_{47} vs. An_0) at low pH. In contrast, (Al,Si) disordering had no discernible effect during the simulations involving the single-layer retreat mechanism. These results suggest that the effect of (Al,Si) disorder on albite dissolution rate is mechanism-dependent.

Keywords: Long-range order, short-range order, disorder, albite, Monte Carlo, dissolution mechanism, kinetics

Introduction

Feldspar is the single most abundant mineral group in the Earth's crust. The varieties of feldspar account for 60% of the Earth's upper crust. Reactions at feldspar-fluid interfaces govern the composition of surface waters, rates of elemental cycling, and maintenance of global CO_2 concentrations through geologic time. In the past, a variety of factors, such as pH, temperature, saturation state, and compositional variation have been investigated in both laboratories and in natural systems to evaluate effects on feldspar-fluid interactions. These studies have contributed to a comprehensive understanding of the nature of feldspar-fluid interactions (see Blum and Stillings 1995 for detailed review). Even when the feldspar compositions, temperature, pH, and fluid chemistry are all similar, however, feldspar dissolution rates have been observed varying by up to three orders of magnitude between different laboratories. Despite the vast literature on feldspar minerals, the roles of aspects such as (Al,Si) disorder in a single feldspar phase, structural, and compositional heterogeneities due to different space groups, dislocations, twin planes, and exsolution lamellae on feldspar-fluid interactions are not well studied. For example, the extent of (Al,Si) order/disorder affects the bulk thermodynamic properties of feldspar (e.g., Myers et al. 1998), and thus may have a quantitative impact on its interaction with surrounding fluids. At the atomic scale, domains that differ in terms of Al,Si distributions can yield distinctly different surface configurations during feldspar weathering due to preferential dissolution of Al (e.g., Jordan et al. 1999). Therefore, analysis of (Al,Si) disorder in feldspar and the evaluation of corresponding controls on dissolution can provide more accurate understanding of the general mechanisms and kinetics of feldspar-fluid interactions.

As an end-member of the feldspar group, albite ($NaAlSi_3O_8$) presents an ideal opportunity to explore the phenomena of (Al,Si) order/disorder and to evaluate its effect on feldspar-fluid interaction. The structure of albite consists of a framework of corner-sharing Si and Al tetrahedra (Fig. 1). In its triclinic structure, there are four sets of similar but unique tetrahedral sites, conventionally labeled T1o, T1m, T2o, T2m (o = center of symmetry, m = mirror plane). The way in which Si and Al atoms are distributed in the T-sites leads to the distinction among different order-disorder configurations (Nesse 2000). Albite has a fully ordered configuration where the T1o sites contain all the Al atoms and T1m, T2o, and T2m sites only contain Si atoms. As the fraction of Al atoms in T1o sites decreases from 1, the albite crystal lattice can exhibit variations in ordering at different length scales (Stewart et al. 1969; Meneghinello et al. 1999). Macroscopically, the variations of Al fractions in the non-equivalent T-sites are reflected in changes to lattice geometry (Stewart et al. 1969; Vinograd et al. 1999). For example, crystal structure analyses of alkali feldspars have shown that the isochemical variations in cell parameters and reciprocal lattice angles are related to Al/Si distribution among the non-equivalent T-sites of the feldspar framework (Stewart et al. 1969). These average properties reflect long-range order of albite (LRO; e.g., Vinograd et al. 1999). X-ray and neutron diffraction techniques are sensitive to changes in the average structure and thus are good tools to recognize LRO in the crystal structure. In addition, variation in local (Al,Si) lattice distributions occurs even when the degree of LRO is constant (i.e., the fractions of Al atoms in the non-equivalent T-sites are fixed), except in fully ordered low albite. Short-range order (SRO) describes correlation between *n*-order neighboring cation site occupancies. The term "*n*-order" refers here to the pairs of atoms in the lattice that are first-, second-, or even higher-order neighbors. For instance, $n = 1$ and $n = 2$ correspond to the pairs of first-nearest and second-nearest neighbors, respectively. Short-range information can be obtained from nuclear magnetic resonance (NMR) experiments. For example,

* E-mail: aluttge@rice.edu

0003-004X/07/0809–1316$05.00/DOI: 10.2138/am.2007.2471

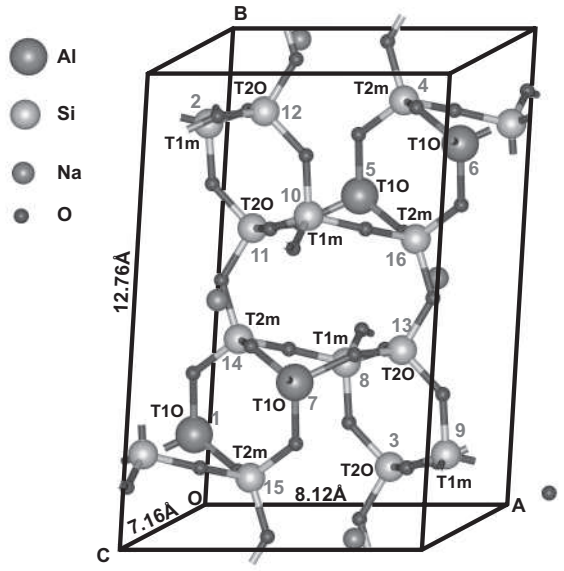

FIGURE 1. Unit cell of low albite. The unit cell contains 16 tetrahedral sites (as numbered), which belong to four non-equivalent sets. Variations of Al and Si distributions in these T-sites yield different degrees of order. The cartoon specifies the fully ordered low albite where Al atoms occupy all T1o sites, and T1m, T1o, and T2m sites contain all the Si atoms.

low albite exhibits three particularly well resolved peaks in ^{29}Si NMR spectra, each of which corresponds to silicon occupation of a given type of T-site (Kirkpatrick 1985). A high-symmetry zeolite with only one crystallographically unique tetrahedral site (T-site) will in general exhibit ^{29}Si NMR spectra with up to five lines, associated with Si having different numbers of aluminum neighbors (m = 0–4) (Peterson 1999).

Manipulation and quantitative analysis of (Al,Si) distribution (e.g., Meneghinello et al. 1999) and experimental evaluation of its effect in albite dissolution kinetics are difficult, and in this respect computer simulations can play a key role. Monte Carlo (MC) methods have been shown to be a powerful tool for both the study of cation distribution in minerals (e.g., Dove et al. 1996; Thayaparam et al. 1996; Lavrentiev et al. 2003; Palin et al. 2003; Sainz-Diaz et al. 2003; Matsumoto et al. 2005) and the simulation of crystal dissolution and growth (e.g., Zhang et al. 1998; Lasaga and Lüttge 2001, 2003, 2004a, 2004b, 2005). In the current study, we utilize Monte Carlo methods to (1) construct albite lattice configurations with different but arbitrary degrees of LRO and SRO, and (2) more importantly implement two different dissolution mechanisms to these configurations for studying the role of (Al,Si) disorder in the dissolution processes of albite.

We hope to convince the reader of the importance of distinguishing LRO and SRO as they relate to dissolution mechanism, and thus we begin by providing detailed working definitions of these terms in the preliminary section below. Because of our extensive use of Monte Carlo techniques, this section also includes a detailed summary of the algorithms employed to drive the simulations. As a means of reducing the difficulty in visualizing order/disorder relationships in three dimensions, we also introduce a compact 2D projection model to show the effect of SRO/LRO variations on actual lattice configurations.

DEFINITIONS OF LRO AND SRO

The long-range order coefficient S is adopted from previous studies (Smith and Brown 1988; Meneghinello et al. 1999) to account for macroscopic Al fractions in these T-sites:

$$S = \sum_{j=1}^{4}[(p_j - P_j)/(1 - P_j)]/4 \quad (1)$$

where p_j is the fractional frequency of an atom in the j^{th} lattice node, obtained by structural refinement [i.e., Al for j = 1 (T1o site) and Si for j = 2, 3, 4 (T1m, T2o, T2m sites, respectively)] and P_j is the occupancy of the same atom in the configuration for which disorder is maximized (i.e., P_1 = 0.25 and $P_2 = P_3 = P_4$ = 0.75 in albite). According to Equation 1, the S parameter is dominated by the Al content of T1o sites. For a given Al content of T1o sites, variation of Al in the other three sets of T-sites correspond to the same S value (Table 1). As the Al content of T1o sites decreases from 1 (in the case of *low* albite) to 0.25 (in fully disordered high albite), the coefficient S decreases subsequently from 1 to 0. Also, S can become negative when the Al content of T1o sites drops below 0.25. The Al content on T1o < 0.25 is not actually observed in nature, but several artifacts with negative S are involved in the current study (Table 1), which, as shown later in this study, do not contradict the general conclusions.

As described in the introduction, the LRO accounts for the majority of ordering in albite. In fact, the albite samples used in dissolution experiments are simply mentioned as high albite or low albite. Therefore, the first motivation in our current study is to study the effect of LRO in the dissolution processes of albite. After the degree of LRO is fixed, we vary SRO to investigate Si enrichment in small sublattices.

Many of the previous studies (e.g., Myers et al. 1998; Palin et al. 2001, 2003) defined SRO as the sum function of pair interactions in the crystal lattice. This strategy fails here as we are investigating isochemical configurations of albite, particularly when the "aluminum avoidance principle" is implemented. In more detail, the main driving force behind (Al,Si) order/disorder in the albite lattice is avoidance of nearest-neighbor Al/Al-neighbors (i.e., Loewenstein's rule in Loewenstein 1954); the direct consequence of such Al-O-Al avoidance in the albite lattice is that the numbers of first-nearest Si-Si, and Si-Al neighbors are constant. For example, in one mole of albite having the formula $NaAlSi_3O_8$, the total number of first-nearest neighbors (i.e., Si-O-Si and Si-O-Al; according to the rule of aluminum avoidance, instances of Al-O-Al are forbidden) is 8 moles. For each Al, there are four Si-O-Al bonds. i.e., the number of Si-O-Al bonds ($N_{Si\text{-}O\text{-}Al}$) in 1 mole of $NaAlSi_3O_8$ is 4 moles. Thus the number of Si-O-Si bonds ($N_{Si\text{-}O\text{-}Si}$) is 4 moles per mole $NaAlSi_3O_8$. As the total numbers of Si-O-Si and Si-O-Al bonds remain constant, if we only consider the first-nearest neighbors various albite configurations differ from each other in the numbers of Si atoms with l first-nearest Si neighbors (i.e., $N_{(Si,l)}$, l = 0–4). For example, in the low albite configuration with S = 1, two thirds of the Si atoms have 3 Si-O-Si and 1 Si-O-Al bonds, and one third of the Si atoms have 2 Si-O-Si and 2 Si-O-Al bonds. When Al atoms disperse from T1o sites to the other three T sites, the resulting high albite configurations can have Si atoms with all possible numbers of Si first-nearest neighbors (l = 0–4), and again, all the Al atoms each have 4 first-nearest Si neighbors.

TABLE 1. Various Al distributions in T-sites of the albite structure and the corresponding LRO, SRO, and dissolution rates

Sample	X_{Al}(T1o)	X_{Al}(T1m)	X_{Al}(T2o)	X_{Al}(T2m)	*S*	(U/U_0)*	$(rate)/(rate)_0$*	(U/U_0)†	$(rate)/(rate)_0$†
1	1.0	0	0	0	1.00	1.0	1.000	1.0	1.000
2	0.9	0.1	0	0	0.87	2.6	1.080	2.0	2.484
3	0.8	0.2	0	0	0.73	4.0	1.194	3.5	2.816
4	0.8	0.1	0.05	0.05	0.73	4.2	1.675	3.6	3.095
5	0.7	0.3	0	0	0.60	5.8	1.233	5.4	2.722
6	0.7	0.1	0.1	0.1	0.60	6.1	2.016	4.9	3.287
7	0.7	0.2	0.05	0.05	0.60	6.1	1.789	4.4	3.472
8	0.6	0.4	0	0	0.47	7.9	1.075	7.6	2.388
9	0.6	0.3	0.05	0.05	0.47	78.8	1.963	4.8	3.434
10	0.6	0.2	0.1	0.1	0.47	8.4	2.421	5.7	4.034
11	0.6	0	0.4	0	0.47	7.7	3.906	7.6	7.783
12	0.5	0.3	0.1	0.1	0.33	11.1	2.816	6.0	3.852
13	0.5	0.3	0.2	0	0.33	11.2	2.887	5.8	4.215
14	0.5	0.4	0.1	0	0.33	10.9	2.243	5.0	3.539
15	0.5	0.5	0	0	0.33	10.3	0.672	10.3	1.045
16	0.4	0.4	0.1	0.1	0.20	11.1	3.013	6.2	4.022
17	0.4	0.5	0.1	0	0.20	10.8	2.148	5.1	3.560
18	0.4	0.2	0.2	0.2	0.20	11.2	3.823	7.1	4.854
19	0.3	0.5	0.1	0.1	0.07	11.1	2.850	6.1	4.155
20	0.3	0.4	0.2	0.1	0.07	11.2	3.457	6.8	4.742
21	0.25	0.25	0.25	0.25	0	11.3	4.182	7.4	5.155
22	0.2	0.4	0.2	0.2	–0.07	11.2	4.057	7.3	5.071
23	0.2	0.3	0.3	0.2	–0.07	11.2	3.752	7.3	5.071
24	0.1	0.3	0.3	0.3	–0.20	11.2	4.000	7.1	5.153

* U/U_0 and $(rate)/(rate)_0$ corresponding to the initial albite configurations before SRO minimization where U_0 is the *U* value of low albite and $(rate)_0$ is the dissolution rate of low albite.
† U/U_0 and $(rate)/(rate)_0$ corresponding to the SRO-minimized albite configurations.

In this study, we define a SRO index as a sum contribution of individual tetrahedral atoms. Rather than use a sum function to quantify the first-order neighboring environment for an individual tetrahedral atom (as discussed above, the use of a sum function can not distinguish different albite configurations as Al-O-Al bonds are not allowed in albite configurations), we introduce a local parameter $U_{\text{individual}}$ with an exponential form:

$$U_{\text{individual}} = \exp(l/2 \cdot U_{\text{Si-O-Si}})\exp[(4-l)/2 \cdot U_{\text{Si-O-Al}}] \quad (2)$$

where l is the number of Si-O-Si bonds and $(4-l)$ is the number of Si-O-Al bonds for a typical tetrahedral atom. For a given tetrahedral atom, $U_{\text{Si-O-Si}}$ and $U_{\text{Si-O-Al}}$ are the individual contributions of Si-O-Si and Si-O-Al bonds, respectively. Proper selection of $U_{\text{Si-O-Si}}$ and $U_{\text{Si-O-Al}}$ values is discussed below.

The SRO parameter U is designated as the sum of the individual contribution of tetrahedral atoms with differing local property:

$$\begin{aligned} U &= \sum U_{\text{individual}} \\ &= N_{\text{Al}} \exp(2 \cdot U_{\text{Si-O-Al}}) + \sum_{l=0}^{4} \{N_{(\text{Si},l)} \exp(l/2 \cdot U_{\text{Si-O-Si}}) \exp[(4-l)/2 \cdot U_{\text{Si-O-Al}}]\} \\ &= N_{\text{Al}} \exp(2 \cdot U_{\text{Si-O-Al}}) + \sum_{l=0}^{4} \{N_{(\text{Si},l)} \exp(2 \cdot U_{\text{Si-O-Al}}) \exp[l/2 \cdot (U_{\text{Si-O-Si}} - U_{\text{Si-O-Al}})]\} \\ &= \exp(2 \cdot U_{\text{Si-O-Al}}) \left\langle N_{\text{Al}} + \sum_{l=0}^{4} \{N_{(\text{Si},l)} \exp[l/2 \cdot (U_{\text{Si-O-Si}} - U_{\text{Si-O-Al}})]\} \right\rangle \end{aligned} \quad (3)$$

In Equation 3, N_{Al} is the number of Al atoms in an albite configuration, and N_{Si} is the number of Si atoms. $N_{(\text{Si},l)}$ represents the number of Si atoms with l first-nearest Si neighbors. U can be treated as a function of 5 independent variables, i.e., $N_{(\text{Si},l)}$, l = 0–4. As discussed above, for each mole of albite ($NaAlSi_3O_8$), N_{Al}, N_{Si}, and $N_{(\text{Si},l)}$ in Equation 3 also satisfy:

$$3N_{\text{Al}} = N_{\text{Si}} = \sum_{l=0}^{4} N_{(\text{Si},l)} = 3N_A \quad (4)$$

and

$$\sum_{l=0}^{4} l \cdot N_{(\text{Si},l)} = 8N_A \quad (5)$$

where N_A is Avogadro's number (6.02×10^{23}). The constraints imposed by Equations 4 and 5 reduce the number of independent variables in Equation 3 to 3. To derive the overwhelming effect of $N_{(\text{Si},4)}$ on the value of U, we define

$$f = \exp(U_{\text{Si-O-Si}} - U_{\text{Si-O-Al}}) \quad (6)$$

and pick sufficiently different values of $U_{\text{Si-O-Si}}$ and $U_{\text{Si-O-Al}}$ such that $f >> 0$. For example, $U_{\text{Si-O-Al}} = 3$ and $U_{\text{Si-O-Si}} = 100U_{\text{Si-O-Al}}$. Equation 3 can then be rewritten as

$$U = \exp(2 \cdot U_{\text{Si-O-Al}}) \left[N_{\text{Al}} + \sum_{l=0}^{4} (N_{(\text{Si},l)} f^{l/2})\right] \quad (7)$$

The minimization of U according to Equation 7 will effectively reduce the number of $N_{(\text{Si},4)}$ in the albite configurations.

The strategy behind this definition of SRO is that a Si atom "rejects" a neighbor of the same type. The existence of Si-rich clusters will exaggerate the uneven Al distribution by increasing $U_{individual}$ exponentially (Eq. 2). As the degree of LRO is fixed, the minimization of U corresponds to the configuration with decreased Si-rich clusters in size.

COMPUTER MODELING

In this study, we defined a network of tetrahedral sites with the same relative positions as in the real crystal. A simulation cell of $20 \times 20 \times 12$ unit cells was used that includes 76 800 T-sites. To avoid artifacts at the boundaries of the simulation cell, we used periodic boundary conditions (PBC). The use of PBC allows the behavior of this relatively small supercell to approximate that of the bulk system.

Al,Si distributions with different LRO

Albite configurations having different LRO were generated by Monte Carlo methods. The total of 24 arbitrary sets of Al distributions on different T-sites are listed in Table 1, corresponding to different values of LRO coefficient *S*. To create a

configuration with a given set of Al contents, the starting configuration was an ideal anorthite structure where Al and Si alternate in the lattice. The Al fraction of any individual T-site is thus 0.50. In other words, there is only one type of T-O-T bond, i.e., Si-O-Al. The typical configuration with a certain set of Al fractions in T-sites [i.e., (a, b, c, d), where $0 \le a, b, c, d \le 1$ and $a + b + c + d = 1$] was created by the following algorithm: (1) Calculate the required number of Al atoms ($N_{Al\rightarrow Si}$) to be replaced by Si in all the four sets of T-sites in the starting anorthite configuration: if the total number of T-sites with the same type in the simulated supercell is denoted as N, then $N_{Al\text{-}T1o} = (0.5 - a)N$, $N_{Al\text{-}T1m} = (0.5 - b)N$, $N_{Al\text{-}T2o} = (0.5 - c)N$, $N_{Al\text{-}T2m} = (0.5 - d)N$, where $N_{Al\rightarrow Si}$ can be negative. Steps 2–4 are repeated in succession for T1o, T1m, T2o, and T2m; (2) If $N_{Al\rightarrow Si} > 0$, randomly select an Al in the typical T-site, and replace it by a Si atom, and at the same time set $N_{Al\rightarrow Si} = N_{Al\rightarrow Si} - 1$; (3) If $N_{Al\rightarrow Si} < 0$, randomly select a Si in the typical T-sites, replace it by an Al atom, and locate Si atoms in its four first-nearest T-neighbors. Recalculate $N_{Al\rightarrow Si}$ for all sets of T-sites; and (4) If $N_{Al\rightarrow Si} = 0$, proceed to the next set of T-sites.

Minimization of SRO

The construction of the above configuration is constrained only by LRO. While keeping Al fractions in the four sets of T-sites constant, we rearranged the (Al,Si) distribution according to the minimization of SRO. As mentioned previously, the purpose of the SRO minimization is to provide an opportunity for pairwise repulsion of Si. The initial values of $U_{Si\text{-}O\text{-}Al}$ and $U_{Si\text{-}O\text{-}Si}$ are defined as:

$$U_{Si\text{-}O\text{-}Al} = 3 \tag{8}$$

$$U_{Si\text{-}O\text{-}Si} = 100U_{Si\text{-}O\text{-}Al} \tag{9}$$

The minimization process proceeds as follows. (1) Calculate U according to Equation 3. (2) Randomly choose a Si atom with 4 Si first-nearest neighbors and an Al atom, both of whom belong to the same set of T-sites. Calculate U associated with the new configuration if the two chosen atoms are exchanged. If U decreases, exchange these two atoms. Otherwise, exchange these two atoms with probability $\exp[-(U_{new} - U_{old})/Z(T)]$ where $Z(T_0)$ is adjusted to satisfy $\exp[-(U_{new} - U_{old})/Z(T_0)] \sim 20\%$. Repeat this step 10^4 times; and (3) $Z(T) = 90\%\ Z(T)$.

Repeat steps 2–3 in a succession until U oscillates slightly around a minimum value. After the SRO minimization process, the values of U in all albite configurations are recalculated by using $U_{Si\text{-}O\text{-}Al} = 3$ and $U_{Si\text{-}O\text{-}Si} = 6$.

Dissolution modeling

We utilized parameterized Monte Carlo methods to simulate the stochastic processes of albite dissolution. To provide clarity, we describe these processes in some detail below.

The dynamics of albite dissolution can be described as a sequence of three basic microscopic events: attachment of solution atoms at empty surface sites, detachment of surface atoms, and diffusion of surface atoms from one surface site to another. At low pH, interstitial cations (Na^+) participate in simple exchange reactions with hydrogen ions. The exchange reaction is relatively fast (Oelkers et al. 1994; Gout et al. 1997; Hellmann et al. 1997; Mukhopadhyay and Walther 2001; Nesbitt et al. 2001) and is thus unlikely to be a rate-limiting step. Under these conditions, albite dissolution is limited by the destruction of the residual tetrahedral framework. The protonation of surface O atoms creates surface silanol (Si-OH), aluminol (Al-OH), or hydroxyl bonds (T-OH-T). Ab initio calculations of various protonated aluminosilicate clusters (Xiao and Lasaga 1994; Kubicki et al. 1996; Sykes et al. 1997) have shown that the protonation weakens the oxygen-bridging bonding of surface tetrahedral atoms. During the dissolution process, a tetrahedrally coordinated surface atom experiences a sequence of events: protonation of the oxygen-bridging bonds, breakage of these protonated bonds, and final transport into the solution. Changes in the tetrahedral coordination of Al atoms also occurs (e.g., Xiao and Lüttge 2002) further complicating the dissolution processes. As our objective here is to simulate the stochastic processes of albite dissolution, we will not dwell on quantum-chemical aspects of these surface reactions. For purposes of simplicity in our Monte Carlo simulations, this stepwise sequence is treated as one detachment event in our model. The frequency of the detachment is expressed as:

$$k_{i,j}^{-} = \nu \exp(-i\frac{\Phi_{SiSi}}{kT})\exp(-j\frac{\Phi_{SiAl}}{kT}) \tag{10}$$

where ν is a frequency factor that defines the time, k is Boltzmann's constant (J/K), and T is the temperature in K. The variables i and j represent the numbers of Si-O-Si and Si-O-Al bonds, respectively. As the detachment of Al occurs, i is set to zero (no Si-O-Si bonds in the case of Al detachment). Φ_{SiSi}/kT and Φ_{SiAl}/kT are the bond energies of Si-O-Si and Si-O-Al, respectively, in units of kT.

At equilibrium, the attachment rate is equal to the detachment rate of atoms from kink sites (e.g., Zhang et al. 1998; Lasaga and Lüttge 2001, 2003, 2004a, 2004b, 2005). When the saturation state of the solution deviates from equilibrium, the attachment rate of tetrahedral atoms from the solution to the crystal surface is exponentially proportional to $\Delta\mu$. As each bulk Al atom has four Al-O-Si bonds in the albite structure, the attachment of an Al atom onto the albite framework is governed by:

$$k_{Al}^{+} = \nu \exp(-2\frac{\Phi_{SiAl}}{kT})\exp(\frac{\Delta\mu_{Al}}{kT}) \tag{11}$$

where $\Delta\mu_{Al}$ is the difference in chemical potential between Al in the solution and in the crystal structure. $\Delta\mu_{Al}$ is related to the concentration of aluminum in the solution, C_{Al} by $C_{Al}/C_{Al,eq} = \exp(\Delta\mu_{Al}/kT)$. On average each bulk Si atom in albite structure has 8/3 Si-O-Si and 4/3 Si-O-Al bonds, therefore the rate constant for the attachment of a Si atom is:

$$k_{Si}^{+} = \nu \exp(-\frac{4}{3}\frac{\Phi_{SiSi}}{kT})\exp(-\frac{2}{3}\frac{\Phi_{SiAl}}{kT})\exp(\frac{\Delta\mu_{Si}}{kT}) \tag{12}$$

where $\Delta\mu_{Si}$ is the difference in chemical potential between Al in the solution and in the crystal structure. $\Delta\mu_{Si}$ is related to the concentration of Si in the solution, C_{Si} by $C_{Si}/C_{Si,eq} = \exp(\Delta\mu_{Si}/kT)$.

In the Monte-Carlo-based dissolution modeling, Φ_{SiSi}/kT, Φ_{SiAl}/kT, $\Delta\mu_{Si}$, and $\Delta\mu_{Al}$ are the four key parameters. Their relative values determine dissolution rates of Si and Al atoms. In our current study, the determination of Φ_{SiSi}/kT and Φ_{SiAl}/kT relies strongly on quantum chemistry calculations. A substantial number of ab initio calculations and density functional theory (DFT) modeling have been conducted in the investigation of aluminosilicate-fluid surface reactions (e.g., Xiao and Lasaga 1994; Kubicki et al. 1996; Sykes et al. 1997; Xiao and Lüttge 2002). Although these calculations cannot quantify the pH effect on the values of Φ_{SiSi}/kT and Φ_{SiAl}/kT, in general it requires more energy to break Si-O-Si bonds relative to Si-O-Al bonds in an acidic pH environment. Xiao and Lüttge (2002) combined solvated ab initio and DFT modeling and further narrowed the range of possible Φ_{SiSi}/kT and Φ_{SiAl}/kT values at low pH. Based on their study, we chose $\Phi_{SiSi}/kT = 6$ and $\Phi_{SiAl}/kT = 3$. This choice has been validated in our Monte Carlo studies of dissolution kinetics of plagioclase feldspars: saturation state, compositional variation, aluminum inhibition, and surface morphologies have all been investigated, and shown to be consistent with experimental measurements and field observations. These aspects of our Monte Carlo-based studies on aluminosilicate dissolution kinetics will be extended in a series of papers.

Albite dissolution rates are low (for a review see Blum and Stillings 1995), and most albite dissolution experiments must be conducted in far-from-equilibrium conditions at high temperature (100–300 °C). Accordingly, the solution concentrations of all dissolved species become vanishingly small in our modeling, i.e., $\Delta\mu_{Si} << 0$ and $\Delta\mu_{Al} << 0$.

To avoid grain size effects in computer simulations of 3-dimensional albite dissolution, we used only a single oriented albite (001) face. Periodic boundary conditions in this kinetic model were applied to the *ab* planar boundaries. To simulate the many-body (stochastic) nature of the dissolution process by Monte Carlo methods, the frequencies of the three basic surface events are converted into possibilities. We define the total frequency (P_t), i.e., the number of all possible events in a unit interval, as:

$$P_t = N_{i,j-}k_{i,j}^{Si-} + N_{j-}k_{j}^{Al-} + N_{i,j+}k_{Si}^{+} + N_{j+}k_{Al}^{+} \tag{13}$$

where $N_{i,j-}$ is the number of Si atoms with i Si-O-Si and j Si-O-Al bonds available for detachment, N_{j-} the number of Al atoms with j Si-O-Al bonds available for detachment, $N_{i,j+}$ the number of empty tetrahedral sites with i first-nearest Si neighbors and j first-nearest Al neighbors available for Si attachment, and N_{j+} the number of empty tetrahedral sites with j first-nearest Si bonds available for Al attachment. The interval (Δt) between two basic events can be expressed as:

$$\Delta t = 1/P_t \tag{14}$$

In this interval, the probabilities of Si and Al detachment are, respectively:

$$P_{Si-} = N_{i,j-}k_{i,j}^{Si-}/P_t \tag{15}$$

$$P_{Al-} = N_{j-}k_{j}^{Al-}/P_t \tag{16}$$

Similarly, the probabilities of Si and Al attachment are, respectively:

$$P_{Si+} = N_{i,j+} k^{+}_{Si} / P_t \quad (17)$$

$$P_{Al+} = N_{j+} k^{+}_{Al} / P_t \quad (18)$$

With the definitions of Equations 9–14, the stochastic algorithm proceeds as follows. (1) Initialization of the system. At dissolution time $t = 0$, the number of dissolved tetrahedral atoms $N_T = 0$. (2) Generate a random number r. (3) If $r < P_{Si-}$, randomly select a surface Si atom and vacate its T-site; $N_T = N_T + 1$. Go to step 7; (4) If $P_{Si-} < r < P_{Si-} + P_{Al-}$, randomly select a surface Al atom and vacate its T-site; $N_T = N_T + 1$. Go to step 7; (5) If $P_{Si-} + P_{Al-} < r < P_{Si-} + P_{Al-} + P_{Si+}$, randomly select an empty surface Si-site and coordinate a Si atom in this T-site; $N_T = N_T - 1$. Go to step 7; (6) If $P_{Si-} + P_{Al-} + P_{Si+} < r < 1$, randomly select an empty surface Al-site and coordinate an Al atom in this T-site; $N_T = N_T - 1$. Go to step 7; (7) Update $N_{i,j-}$, N_{j-}, $N_{i,j+}$, N_{j+}, and N_T; (8) Increment elapsed time as $t = t + \Delta t$.

Steps 2–8 are repeated in succession until a certain number of tetrahedral atoms are dissolved or precipitated. In the algorithm, the net number of dissolved tetrahedral atoms (N_T) is recorded periodically together with the elapsed time (t). This enables us to calculate the dissolution rate of albite in the dissolution process. In the current study, the dissolution rate is normalized to the surface geometry area and thus has the units of [mol/m^2/(1/v)].

Visualization of site ordering: A 2D projection model

To reduce the difficulty in visualizing order/disorder relationships in three dimensions, we introduce a compact 2D projection model to show the effect of SRO/LRO variations on actual lattice configurations. In this model, the unit cell of albite is projected to the *ab* plane and rearranged into a 4 × 4 matrix. In Figure 2, the unit cell of 16 tetrahedral sites is enclosed by a gray dashed frame. The four types of non-equivalent T sites have been distinguished by shading. T1o, T1m, T2o, and T2m sites are denoted as white circles, dark gray circles, medium gray circles, and light gray circles, respectively. Also, these tetrahedral sites have been numbered to denote their relative positions and their corresponding 3D positions can be found in Figure 1. With this projection model, an albite configuration can be visualized as a sequence of 2D square lattices, each of which represents a (001) layer of one unit cell in height.

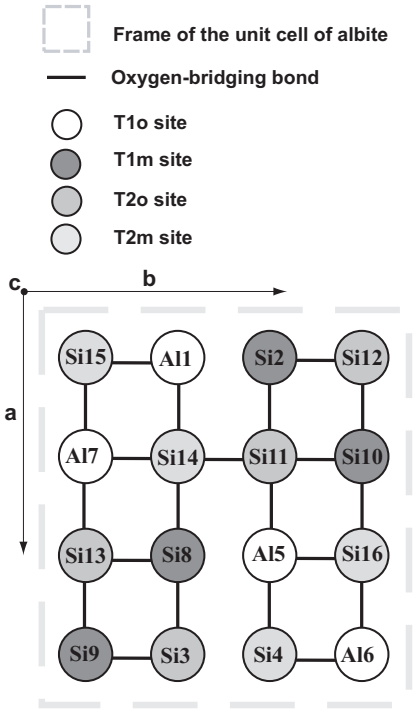

FIGURE 2. The 2D projection model: the 16 tetrahedral sites in the unit cell of albite (Fig. 1) are projected onto the *ab* plane and are rearranged into a 4 × 4 matrix. In the 2D unit cell, the tetrahedral sites are numbered and their corresponding 3D positions can be found in Figure 1. By using the 2D projection model, a (001) layer of albite configuration can be modeled as a square lattice.

RESULTS AND DISCUSSION

Configurations

Pairs of SRO and LRO indices, U and S, corresponding to typical configurations before and after SRO minimizations, are shown in Figure 3. Low albite with $S = 1$ has the minimum value of U, which is referred to as U_0 below. Prior to SRO minimization (gray squares in Fig. 3), U/U_0 increases linearly from 1 to ~11 when S decreases from 1 to ~0.33; as S is less than 0.33, U/U_0 remains constant at ~11. The correlation of U with S indicates that sublattices become more enriched in Si as more Al atoms disperse from T1o sites to the other three sets of T-sites. After a minimum of 50% T1o sites are occupied by Si atoms, the uneven Al/Si distribution is saturated. A similar correlation of U with S is also displayed for the configurations after SRO minimization. As shown by black diamonds in Figure 3, U/U_0 increases linearly from 1 to ~6, when S decreases from 1 to ~0.6. In the S range of [–0.20, 0.6], U/U_0 values vary between 6 and 7.

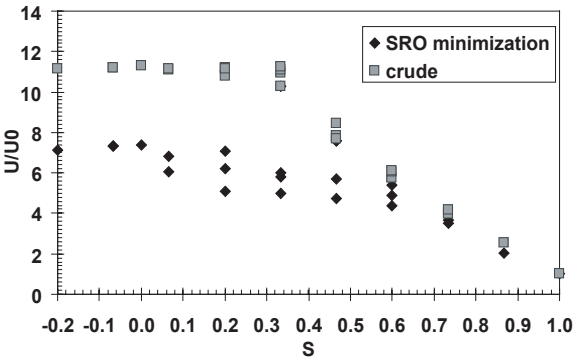

FIGURE 3. Pairs of SRO and LRO indices, U and S, corresponding to typical configurations before and after SRO minimization.

Comparison of the two sets of configurations before and after SRO minimizations indicates that the minimization reduces the incidence of Si clusters. Shown in Figure 3, all the SRO-minimized configurations, except low albite, have a decrease in U relative to their corresponding crude configurations. A bigger drop of U corresponds to a smaller S value.

The effect of the minimization of U is shown by projection of the configurations. We first applied the 2D projection model to the 24 initial configurations, 10 of which are shown in Figures 4a–4j. In Figure 4, each square lattice represents a one unit cell high (001) layer randomly chosen from a typical configuration. In these lattices, Al atoms are denoted by black squares. Configurations with different LRO exhibit different texture patterns. For example, low albite possesses a well-organized texture in Figure 4a. Dispersions of Al from T1o into the other three sets of T-sites gradually replace this pattern with more diverse textures (Figs. 4b–4j). For instance, the exclusive dispersion of Al into T2o sites results in the texture with horizontal stripes (Fig. 4f). The texture with perfect vertical stripes (Fig. 4h) stands for the configuration that apportions Al equally between T1o and T1m

sites. As a mixture of these two types of Al distributions, the configuration in Figure 4g also exhibits a fairly well-organized texture. The rest of the configurational textures are relatively poorly organized, with irregular distributions of Si-rich sublattices visible as small white irregularly shaped domains.

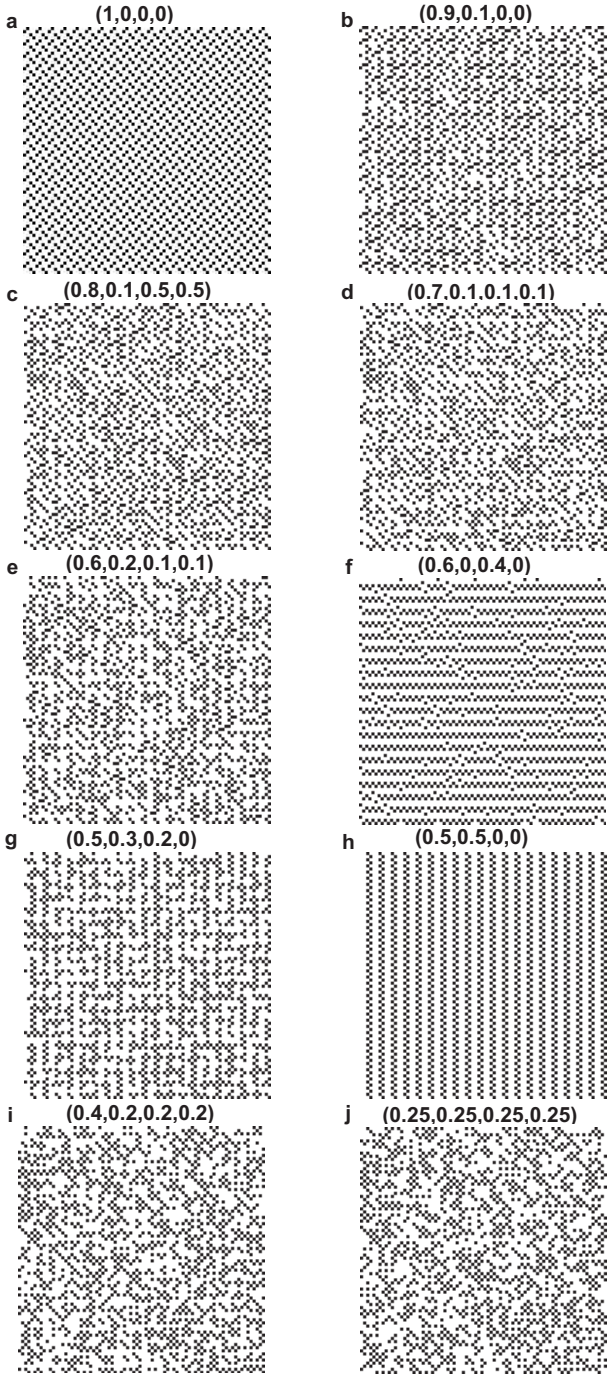

FIGURE 4. Different albite configurations before SRO minimization illustrated by the 2D projection model. Each square lattice represents a (001) layer of a typical albite configuration where 20 × 20 unit cells are involved. Aluminum atoms are represented by black dots in the lattice, whereas Si atoms are represented by white dots. The four numbers in the bracket above a square lattice indicate Al fractions in T1o, T1m, T2o, and T2m, respectively.

Figure 5 illustrates 8 SRO-minimized configurations. As low albite has zero freedom for SRO minimization, its configuration remains unchanged (Fig. 5a and 4a). The other seven configurations (Figs. 5b–5h) have more random Al distributions relative to their corresponding crude configurations (Fig. 4). For example, the special pattern in Figure 5f has changed dramatically from that in Figure 4g, yielding a random texture. As mentioned previously, our current SRO definition only takes into account the minimization of the number of Si atoms with four first-nearest Si-O-Si bonds. As a result, the configurations such as that shown in Figure 5 have not yet eliminated all the Si-rich sublattices. As suggested by Vinograd et al. (2001), the optimization of albite configuration is favored by the consideration of second-nearest neighbors. This effect is not investigated in the current model, as we did not introduce SRO parameters for pairs of second-nearest neighbors.

Role of order/disorder in albite dissolution

Dissolution modeling was carried out on both the two sets of configurations. The modeling results show that the dissolution rates differ as a function of LRO and SRO. The data of $(rate)/(rate)_0$ are plotted vs. S in Figure 6 where $(rate)_0$ denotes the dissolution rate of low albite (Table 1). For the 24 initial configurations, their dissolution rates generally increase with the decrease of S. As listed in Table 1, the configuration of S = 0 has a dissolution rate 3.2 times greater than low albite. After SRO minimization, there is a universal increase in dissolution rates (shown as black diamonds in Fig. 6). For example, the SRO-minimized configuration of S = 0 has a dissolution rate 5.2 times of that of low albite. The universal increase in dissolution rates after SRO-minimization is due to the decrease in the size of Si-rich clusters. The presence of Si-rich clusters retards albite dissolution because the energy required to break a Si-O-Si bond is much higher than required to break a Si-O-Al bond. The increase in the number of Si-O-Si bonds that must be broken to release a surface Si atom increases the energy barrier exponentially. With a fixed degree of LRO, a configuration with a lower degree of SRO has a more regular distribution of Al and Si and therefore a larger dissolution rate.

The variations in dissolution rates for different configurations (Fig. 6) show that the role of Al order/disorder on albite dissolution is significant. For example, the dissolution rate of high albite can be as much as 5× that of low albite. To account for the effect of order/disorder, the Al-content dependence of dissolution rates of plagioclase feldspar was calculated. Here we have used the log-linear dependence of the dissolution rate of plagioclase feldspar on anorthite content observed by Blum and Stillings (1995): $\log(rate) \sim aX_{An}$ (X_{An}: the anorthite content of the plagioclase feldspar) where a = 1.2~2.0 at acidic pH in the X_{An} range of [0, 0.7]. An average value of a = 1.5 results in An_{47} having 5 times the dissolution rate of low albite. Another comparison can be made with the pH dependence of albite dissolution: $\log(rate) \sim -0.49$ pH in the pH range of [1, 5] (Blum and Stillings 1995 and references therein). The fivefold increase in the dissolution rate of albite corresponds to a decrease in pH value by 1.42.

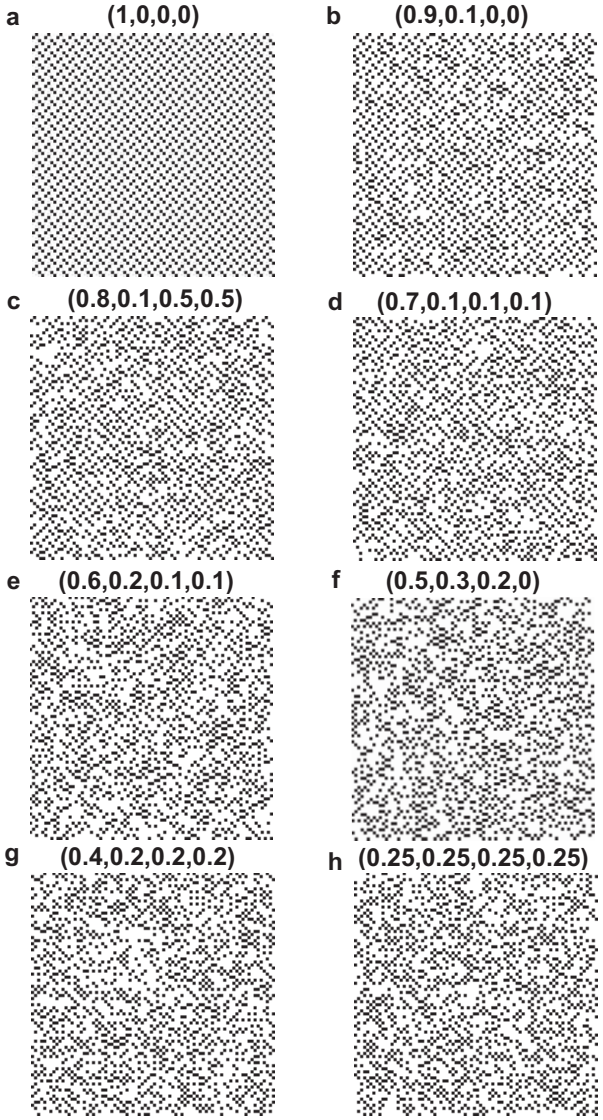

FIGURE 5. Different albite configurations after SRO minimization. Each square lattice represents a (001) layer of a typical albite configuration where 20 × 20 unit cells are involved. Aluminum atoms are represented by black dots in the lattice, whereas Si atoms are represented by white dots. The four numbers in the bracket above a square lattice indicate Al fractions in T1o, T1m, T2o, and T2m, respectively.

The evaluation of order/disorder effects can provide insight to the feldspar dissolution mechanism. The current debate over the dissolution mechanism under acidic conditions focuses on whether feldspar dissolution occurs by multilayer leaching or layer-by-layer retreat. In many experimental studies, the thick altered layer above the feldspar substrate has been considered as a leached layer, formed by preferential dissolution of aluminum (Hellmann et al. 1997; Oelkers et al. 2001; Nesbitt et al. 2001). On the other hand, consistent with the mechanism of layer-by-layer retreat, recent microscopic observations on the surface structure (Jordan et al. 1999; Teng et al. 2001; Fenter et al. 2003a, 2003b; Hellmann et al. 2003) have shown that the

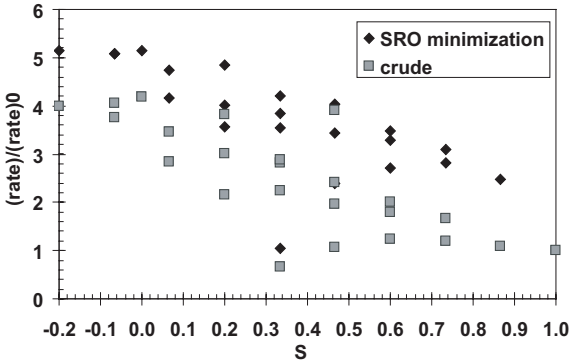

FIGURE 6. In the control of multilayer leaching, the resultant data of $(rate)/(rate)_0$ are plotted vs. S where $(rate)_0$ denotes the dissolution rate of low albite. For the 24 initial configurations, $(rate)/(rate)_0$ increases with the decrease of S. The configuration of $S = 0$ has the dissolution rate 4.2 times greater than low albite. After SRO minimization, there is a universal increase in $(rate)/(rate)_0$. The SRO-minimized configuration with $S = 0$ has its dissolution rate 5.2 times of that of low albite.

altered layer more closely resembles a reprecipitated phase, below which monolayer surface features prevail in the defect-free terrace areas. The coexistence of a reprecipitated phase and the undergoing dissolution on the top of the feldspar substrate is attributed by the mechanism of layer-by-layer retreat to the solution, which is oversaturated with respect to the reprecipitated phase but undersaturated with respect to feldspar. The porous structure of the reprecipitated phase provides an unimpeded transport channel for the feldspar dissolution below. We believe that the investigation of the role of order/disorder in these two competing models will provide insight into a better understanding of feldspar dissolution. Our kinetic results associated with the dissolution modeling described earlier in this study have been based on the mechanism of multilayer leaching. Multilayer leaching occurs when Al atoms dissolve much faster than Si atoms (recall that $\Phi_{SiSi}/kT = 6$ and $\Phi_{SiAl}/kT = 3$), and thus any under-coordinated tetrahedral atoms can be involved in the dissolution processes regardless of their depth in the bulk structure. As shown previously, disordered (Al,Si) distribution under the process of multilayer leaching creates a large potential variability in the determination of the dependence of feldspar dissolution on the anorthite content and pH.

To test the dissolution mechanism of layer-by-layer retreat, we extended the dissolution simulation further to confine the dissolution to the uppermost single layer. In this case, Equation 10 is replaced by:

$$k_{i,j}^{\mathrm{Si}-} = \nu \cdot e^{-i\frac{\Phi_{\mathrm{SiSi}}}{kT}} e^{-i\frac{\Phi_{\mathrm{SiAl}}}{kT}} e^{-h\frac{\Psi_d}{kT}} \tag{19}$$

$$k_{j}^{\mathrm{Al}-} = \nu \cdot e^{-j\frac{\Phi_{\mathrm{SiAl}}}{kT}} e^{-h\frac{\Psi_d}{kT}} \tag{20}$$

These two equations represent the detachment frequencies of Si atoms and Al atoms, respectively. The index h denotes the layer relative to the uppermost surface layer, and ψ_d is the diffusion barrier coefficient. We set the value for ψ_d equivalent to the bond energy, to confine the dissolution to the uppermost layer. As a result, under-coordinated tetrahedra other than those

in the uppermost layer would encounter a large energy barrier to release into solution. As a result, the dissolution rates observed for the 24 initial configurations converge (Fig. 7). There are no significant differences in the dissolution rates, even between high albite with $S = 0$ and low albite with $S = 1$. Therefore, under the mechanism of layer-by-layer retreat, there is no strong effect of Al,Si order/disorder on the dissolution of albite.

The effect of Al,Si order/disorder differs so strongly in the two dissolution mechanisms that it becomes a unique indicator of albite dissolution mechanism. Unfortunately, there have been few direct investigations of such an effect. In the past, significant efforts have been made in evaluating the dependences of the feldspar dissolution on ΔG, pH, ionic strength, and anorthite content. The majority of these studies, combined with our current study, imply that the dissolution of feldspar is dominated by the layer-by-layer retreat mechanism. For example, despite the diversity of experimental materials, a collection of data from many K-feldspar dissolution studies showed a distinctly linear relationship between log(*rate*) and pH under acidic conditions (Chou and Wollast 1985; Manley and Evans 1986; Schweda 1989; Casey et al. 1991; Oxburgh et al. 1994; Stillings and Brantley 1995; for a review, see Blum and Stillings 1995). Blum and Stillings (1995) concluded that at the same pH, the plagioclase kinetic data from different laboratories roughly follows the same anorthite-dependence trend. Furthermore, the anorthite-content dependence of the feldspar dissolution at acidic pH is characterized by a transitional point around An_{71}—any plagioclase component with $An_{<71}$ has a linear relation of its log(*rate*) to the anorthite content and any plagioclase component with $An_{>71}$ has a bigger dissolution rate than extrapolated from the linear relation (Blum and Stilings 1995). In our computer simulation investigations of plagioclase dissolution kinetics (Zhang and Lüttge, submitted), we found that only the single-layer retreat mode can generate the transitional point.

Concluding remarks

Our main objective was to explore the influence of (Al,Si) order/disorder in the dissolution of albite. We adopted the traditional LRO coefficient S to quantify long-range disorder. As the Al fraction in T1o is known, the value of S is thus uniquely determined. However, because of the local variation in (Al,Si) distributions, a single S value can correspond to multiple albite configurations. Therefore, we introduced a new SRO parameter, U, with an exponential form to quantify the first-nearest Si-Si enrichment. By minimizing U, we were able to minimize the Si enrichment in local sublattices.

Our dissolution modeling results show that the role of (Al,Si) order/disorder in albite dissolution is mechanism-dependent. If multilayer leaching is the dominant dissolution mechanism, the effect of Al,Si order/disorder can be comparable to the effects of pH and anorthite content on the dissolution of feldspar. On the other hand, the layer-by-layer retreat model does not show this relationship, and all the investigated albite configurations have similar dissolution rates. In the context of previous studies on feldspar dissolution, these results strongly imply that the layer-by-layer retreat mechanism dominates the dissolution of feldspar.

The kinetics of feldspar dissolution is a complex issue. Although our kinetic model introduces significant simplifications, its efficiency has been demonstrated from various aspects. More correlated laboratory studies and fieldwork would also be useful. Lastly, we note that our results are based on a limited system size. MC simulations with larger system sizes could be performed to evaluate finite-size effects.

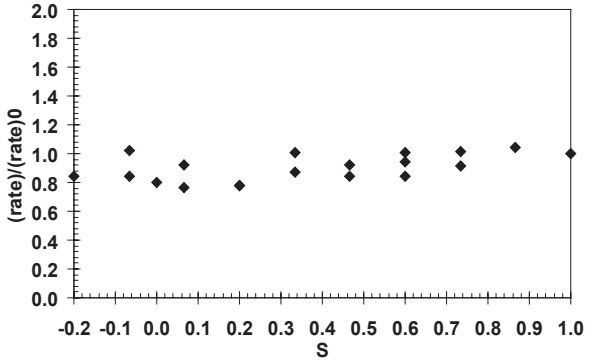

Figure 7. In control of layer-by-layer retreat, the resultant data of $(rate)/(rate)_0$ are plotted vs. S where $(rate)_0$ denotes the dissolution rate of low albite. For the 24 initial configurations, there are no significant differences in the dissolution rates, even between high albite with $S = 0$ and low albite with $S = 1$.

Acknowledgments

We thank Rolf S. Arvidson for his careful review of the manuscript and constructive suggestions, and Antonio C. Lasaga for suggestions and corrections, which highly improved the quality of the manuscript. We thank associate editor Steven R. Higgins and three anonymous reviewers for suggestions and corrections, which enhanced the quality of the manuscript. We gratefully acknowledge support for NSF and DOE.

References cited

Blum, A.E. and Stilings, L.L. (1995) Feldspar Dissolution Kinetics. In A.F. White and S.L. Brantley, Eds., Chemical weathering rates of silicate minerals, 31, p. 291–352. Reviews In Mineralogy, Mineralogical Society of America, Chantilly, Virginia.

Casey, W.H., Westrich, H.R., and Holdren, G.R. (1991) Dissolution rates of plagioclase at pH = 2 and 3. American Mineralogist, 76, 211–217.

Chou, L. and Wollast, R. (1985) Steady-state kinetics and dissolution mechanisms of albite. American Journal of Science, 285, 963–993.

Dove, M.T. and Heine, V. (1996) The use of Monte Carlo methods to determine the distribution of Al and Si cations in framework aluminosilicates from ^{29}Si MAS NMR data. American Mineralogist, 81, 39–44.

Fenter, P., Park, C., Cheng, L., Zhang, Z., Krekeler, M.P.S., and Sturchio, N.C. (2003a) Orthoclase dissolution kinetics probed by in situ X-ray reflectivity: Effects of temperature, pH, and crystal orientation. Geochimica et Cosmochimica Acta, 67, 197–211.

Fenter, P., Cheng, L., Zhang, Z., and Sturchio, N.C. (2003b) Structure of the orthoclase (001)- and (010)-water interfaces by high-resolution X-ray reflectivity. Geochimica et Cosmochimica Acta, 67, 4267–4275.

Gout, R., Oekers, E.H., Schott, J., and Zwick, A. (1997) The surface chemistry and structure of acid-leached albite: New insights on the dissolution mechanism of the alkali feldspars. Geochimica et Cosmochimica Acta, 61, 3013–3018.

Hellmann, R., Dran, J.-C., and Della Mea, G. (1997) The albite-water system: Part III. Characterization of leached and hydrogen-enriched layers formed at 300 °C using MeV ion beam techniques. Geochimica et Cosmochimica Acta, 61, 1575–1594.

Hellmann, R., Penisson, J.-M., Hervig, R.L., Thomassin, J.-H., and Abrioux, M.-F. (2003) An EFTEM/HRTEM high-resolution study of the near surface of labradorite feldspar altered at acid pH: evidence for interfacial dissolution-reprecipitation. Physics and Chemistry of Minerals, 30, 192–197.

Jordan, G., Higgens, S.R., Eggleston, C.M., Swapp, S.M., Janney, D.E., and Knauss, K.G. (1999) Acidic dissolution of plagioclase: In-situ observations by hydrothermal atomic force microscopy. Geochimica et Cosmochimica Acta, 63, 3183–3191.

Kirkpatrick, R.J. (1985) High resolution solid-state sodium-23, aluminum-27, and

silicon-29 nuclear magnetic resonance spectroscopic reconnaissance of alkali and plagioclase feldspars. American Mineralogist, 70, 106–123.
Kubicki, J.D., Blake, G.A., and Apitz, S.E. (1996) Ab initio calculations on aluminosilicate Q_3 species: Implications for atomic structures of mineral surfaces and dissolution mechanisms of feldspars. American Mineralogist, 81, 789–799.
Lasaga, A.C. and Lüttge, A. (2001) Variation of crystal dissolution rate based on a dissolution stepwave model. Science, 291, 2400–2404.
——— (2003) A model for crystal dissolution. European Journal of Mineralogy, 15(4), 603–615.
——— (2004a) Mineralogical approaches to fundamental crystal dissolution kinetics. American Mineralogist, 89, 527–540.
——— (2004b) Mineralogical approaches to fundamental crystal dissolution kinetics—Dissolution of an A_3B structure. European Journal of Mineralogy, 16, 713–729.
——— (2005) Kinetic justification of the solubility product: Application of a general kinetic dissolution model. Journal of Chemical Physics B, 109, 1635–1642.
Lavrentiev, M.Y., Purton, J.A., and Allan, N.L. (2003) Ordering in spinels—a Monte Carlo study. American Mineralogist, 88, 1522–1531.
Loewenstein, W. (1954) The distribution of aluminum in the tetrahedra of silicates and aluminates. American Mineralogist, 39, 92–95.
Manley, P. and Evans, L.J. (1986) Dissolution of feldspars by low-molecular weight aliphatic and aromatic acids. Soil Science, 141, 106–112.
Matsumoto, K., Irisawa, T., Kitamura, M., Yokoyama, E., Kumagai, Y., and Koukitu, A. (2005) Effecitve distribution coefficients of an ideal solid solution crystal: Monte Carlo simulation. Journal of Crystal Growth, 276, 635–642.
Meneghinello, E., Alberti, A., and Cruciani, G. (1999) Order-disorder process in the tetrahedral sites of albite. American Mineralogist, 84, 1144–1151.
Mukhopadhyay, B. and Walther, J.V. (2001) Acid-base chemistry of albite surfaces in aqueous solutions at standard temperature and pressure. Chemical Geology, 174, 415–443.
Myers, E.R., Heine, V., and Dove, M.T. (1998) Thermodynamics of Al/Al avoidance in the ordering of Al/Si tetrahedral framework structures. Physics and Chemistry of Minerals, 25, 457–464.
Nesbitt, H.W. and Skinner, W.M. (2001) Early development of Al, Ca and Na compositional gradients in labradorite leached in pH 2 HCl solutions. Geochimica et Cosmochimica Acta, 65, 715–727.
Nesse, W.D. (2000) Introduction to Mineralogy, p. 208–212. Oxford University Press, U.K.
Oelkers, E.H. (2001) General kinetic description of multioxide silicate mineral and glass dissolution. Geochimica et Cosmochimica Acta, 65, 3703–3719.
Oelkers, E.H. and Schott, J. (1994) The effect of aluminum, pH, and chemical affinity on the rates of aluminosilicate dissolution reactions. Geochimica et Cosmochimica Acta, 58, 2011–2024.
Oxburgh, R., Drever, J.I., and Sun, Y.T. (1994) Mechanism of plagioclase dissolution in acid solution at 25 °C. Geochimica et Cosmochimica Acta, 58, 661–669.
Palin, E.J., Dove, M.T., Redfern, S.A.T., Bosenick, A., Sainz-Diaz, C.I., and Warren, M.C. (2001) Computational study of tetrahedral Al-Si ordering in muscovite. Physics and Chemistry of Minerals, 28, 534–544.
——— (2003) Computational study of tetrahedral Al-Si and octahedral Al-Mg ordering in phengite. Physics and Chemistry of Minerals, 30, 293–304.
Peterson, B.K. (1999) A simulated annealing method for determining atomic distributions from NMR data: silicon and aluminum in faujasite. Journal of Physical Chemistry, 103B, 3145–3150.
Sainz-Diaz, C.I., Palin, E.J., Dove, M.T., and Hernandez-Laguna, A.H. (2003) Monte Carlo simulations of ordering of Al, Fe, and Mg cations in the octahedral sheet of smectites and illites. American Mineralogist, 88, 1033–1045.
Schweda, P. (1989) Kinetics of alkali feldspar dissolution at low temperature. In D.L. Miles, Ed., Proceedings of the 6th International Symposium on Water-Rock Interaction. AA Balkema, Rotterdam, p. 609–612.
Smith, J.V. and Brown, W.L. (1988) Feldspar Minerals, 1, 828 p. Springer-Verlag, Berlin.
Stewart, D.B. and Ribbe, P.H. (1969) Structural explanation for variations in cell parameters of alkali feldspars with Al/Si ordering. American Journal of Science, 267A, 444–462.
Stillings, L.L. and Brantley, S.L. (1995) Feldspar dissolution at 25 °C and pH 3: Reaction stoichiometry and the effect of cations. Geochimica et Cosmochimica Acta, 59, 1483–1496.
Sykes, D., Kubicki, J.D., and Farrar, T.C. (1997) Molecular orbital calculation of ^{27}Al and ^{29}Si NMR parameters in Q3 and Q4 aluminosilicate molecules and implications for the interpretation of hydrous aluminosilicate glass NMR spectra. Journal of Physical Chemistry, 101, 2715–2722.
Teng, H.H., Fenter, P., Cheng, L., and Sturchio, N.C. (2001) Resolving orthoclase dissolution processes with atomic force microscopy and X-ray reflectivity. Geochimica et Cosmochimica Acta, 65, 3459–3474.
Thayaparam, S., Heine, V., Dove, M.T., and Hammonds, K.D. (1996) A computational study of Al/Si ordering in cordierite. Physics and Chemistry of Minerals, 23, 127–139.
Vinograd, V.L. and Putnis, A. (1999) The description of Al,Si ordering in aluminosilicates using the cluster variation method. American Mineralogist, 84, 311–324.
——— (2001) A two-dimensional spin model of Al/Si order in feldspars: visualization of short-range and long-range order. European Journal of Mineralogy, 13, 273–288.
Xiao, Y.T. and Lasaga, A.C. (1994) Ab initio quantum mechanical studies of the kinetics and mechanisms of silicate dissolution: H^+ (H_3O^+) catalysis. Geochimica et Cosmochimica Acta, 58, 5379–5400.
——— (2002) Solvated ab initio and density functional theory (DFT) modeling of mineral-fluid surface reactions: Towards a better understanding of aluminosilicate dissolution mechanisms. GSA 2002 Fall meeting, Denver, Colorado (October 27–30, 2002).
Zhang, J.W. and Nancollas, G.H. (1998) Kink density and rate of step movement during growth and dissolution of an AB crystal in a nonstoichiometric solution. Journal of Colloid and Interface Science, 200, 131–145.

Manuscript received October 5, 2006
Manuscript accepted May 9, 2007
Manuscript handled by Steven Higgins